Dalton Transactions

PAPER

View Article Online
View Journal | View Issue

Published on 02 February 2015. Downloaded by California Institute of Technology on 14/01/2016 23:12:30.

Cite this: *Dalton Trans.*, 2015, **44**, 6767

Thermoelectric properties of the Zintl phases $Yb_5M_2Sb_6$ (M = Al, Ga, In)

Umut Aydemir,*[a] Alex Zevalkink,[b] Alim Ormeci,[c] Heng Wang,[a] Saneyuki Ohno,[a] Sabah Bux[b] and G. Jeffrey Snyder[a]

Received 10th December 2014,
Accepted 29th January 2015

DOI: 10.1039/c4dt03773a

www.rsc.org/dalton

Zintl compounds with chemical formula $Yb_5M_2Sb_6$ (M = Al, Ga, and In) form one of two known $A_5M_2Pn_6$ structure types characterized by double chains of corner-linked MPn_4 tetrahedra bridged by Pn_2 dumbbells. High temperature electronic and thermal transport measurements were used to characterize the thermoelectric properties of $Yb_5M_2Sb_6$ compounds. All samples were found to exhibit similar high p-type carrier concentrations, low resistivity and low Seebeck coefficients in agreement with the band structure calculations. These results, combined with previous studies, suggest that $Yb_5M_2Sb_6$ compounds are semimetals (*i.e.*, they lack an energy gap between the valence and conduction bands), in contrast to the semiconducting alkaline earth (Ca, Sr, Ba) and Eu based $A_5M_2Sb_6$ compounds. $Yb_5M_2Sb_6$ compounds have very low lattice thermal conductivity, comparable to other closely related $A_5M_2Sb_6$ and A_3MSb_3 phases. However, due to the semimetallic behaviour, the figure of merit of investigated samples remains low ($zT < 0.15$).

Introduction

The thermoelectric efficiency of a material is governed by its figure of merit ($zT = \alpha^2T/\rho\kappa$). High efficiency is typically obtained in heavily doped semiconductors that simultaneously possess a large Seebeck coefficient (α), low electrical resistivity (ρ), and low thermal conductivity (κ).[1,2] Zintl compounds have emerged recently as a promising class of materials for thermoelectric applications.[3,4] These phases are composed of electropositive cations (alkali, alkaline-earth or rare-earth) that donate their valence electrons to anions, which in turn form covalent bonds to satisfy valence requirements.[5] Their complex crystal structures lead to low lattice thermal conductivity and provide opportunities for targeted chemical substitutions to tune the electronic and thermal properties.[6–12]

Within $A_5M_2Pn_6$ Zintl phases (A = Ca, Sr, Ba, Eu, Yb, M = Al, Ga, In, and Pn = As, Sb, Bi), promising zT values have been achieved in several antimonides.[13–15] Two closely related structure types are formed by $A_5M_2Pn_6$ compounds, represented by the prototypical compounds, $Ca_5Ga_2As_6$ and $Ca_5Al_2Bi_6$ (Fig. 1).[16,17] In both structures, corner-sharing chains of MPn_4 tetrahedra are bridged by Pn_2 dumbbells to form infinite, parallel double chains ("ladders"). The primary distinguishing feature between the two $A_5M_2Pn_6$ structure types is in the packing geometry of the ladders. Zintl counting in these anionic double chains yields two Pn^{-1} bridging across the chains, two Pn^{-1} from the corner-sharing tetrahedra, and two Pn^{-2} that are only bonded to M. The two M atoms are each bound to four Pn atoms, yielding a formal valence of −1. The $5A^{+2}$ atoms are situated between the chains, providing overall Zintl charge balance of $[A^{2+}]_5[(4b)M^-]_2\,[(2b)Pn^-]_4[(1b)Pn^{2-}]_2$.

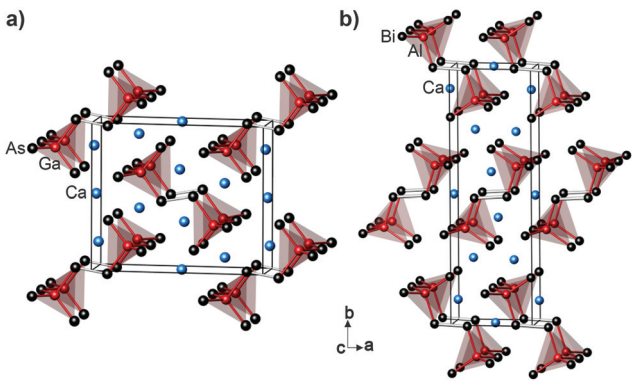

Fig. 1 The crystal structures of (a) $Ca_5Ga_2As_6$ and (b) $Ca_5Al_2Bi_6$ with double chains of different packing geometry.

Representatives of the $Ca_5Ga_2As_6$ structure type include $Ca_5M_2Sb_6$ with M = Al, Ga, and In and $A_5In_2Sb_6$ with A = Sr, Ba, or Eu. All of the compounds with this structure type appear to be semiconducting with band gaps ranging from

[a]*Department of Applied Physics and Materials Science, California Institute of Technology, 1200 E California Blvd, Pasadena, USA. E-mail: uaydemir@caltech.edu*
[b]*Thermal Energy Conversion Technologies Group, Jet Propulsion Laboratory, 4800 Oak Grove Drive, Pasadena, USA*
[c]*Max Planck Institute for Chemical Physics of Solids, Nöthnitzer Str. 40, Dresden, Germany*

Published on 02 February 2015. Downloaded by California Institute of Technology on 14/01/2016 23:12:30.

0.3–0.6 eV.[18–20] In this structure type, the carrier concentrations can be controlled by doping, leading to promising thermoelectric properties.[13–15,21,22] The second structure type ($Ca_5Al_2Bi_6$) is formed by several bismuthides and by the title compounds, $Yb_5M_2Sb_6$, where M = Al, Ga or In.[23–25] Previous reports of the resistivity in $Yb_5In_2Sb_6$ and $Yb_5Al_2Sb_6$ revealed metallic behaviour indicative of either very high defect concentrations or of a semimetallic electronic structure.[23,25] In contrast, a recent investigation of the Ga analogue shows some evidence for semiconducting behavior.[24]

In an attempt to resolve these conflicting reports and to present a comprehensive picture of the thermoelectric properties of this series, the current study investigates the high temperature electronic and thermal transport properties of the three $Yb_5M_2Sb_6$ compounds (M = Al, Ga, In) concurrently. The results of electronic structure calculations and chemical bonding analyses are also reported.

Experimental procedures

Synthesis.

$Yb_5M_2Sb_6$ (M = Al, Ga, and In) samples were synthesized by ball milling followed directly by hot pressing. GaSb and InSb were synthesized as precursors by heating the elements in quartz ampoules up to 600 °C and 800 °C, respectively. After annealing for 12 h at these temperatures, the ampoules were cooled to room temperature in 6 h. Stoichiometric amounts of small-cut Yb ingot (99.9, Alfa Aesar), Sb shot (99.999% Alfa Aesar) and either Al shot (99.999%, Alfa Aesar), GaSb or InSb were loaded under argon into stainless-steel vials with 1/2 inch stainless-steel balls. The contents were ball-milled for 1 h using a SPEX Sample Prep 8000 Series Mixer/Mill. The resulting fine powder was hot-pressed in high-density graphite dies (POCO) under argon using a maximum pressure and temperature of 45 MPa and 550 °C, respectively, for 1 h. The samples were cooled down to room temperature slowly under no load.

Characterization

X-ray diffraction (XRD) was performed on either polished polycrystalline samples or powdered materials using a Philips XPERT MPD diffractometer with reflection mode (Cu-Kα radiation). The lattice parameter determination using α-Si as internal standard and Rietveld refinements were performed by WinCSD program package.[26] Scanning electron microscopy (SEM) and energy dispersive X-ray spectroscopy (EDXS) were performed using a Zeiss 1550 VP SEM. Microprobe analysis with wavelength dispersive X-ray spectroscopy (WDXS, JEOL JXA – 8200 system) was carried out to determine the chemical composition of $Yb_5Al_2Sb_6$ phase. High temperature electronic and thermal transport properties were characterized up to 873 K under dynamic vacuum. The Seebeck coefficients were measured by using Chromel-Nb thermocouples.[27] Hall coefficients and resistivity (Van der Pauw, 4-point probe) were measured simultaneously using a 1 T magnet with tungsten pressure contacts.[28] A Netzch LFA 457 was used to measure the thermal diffusivity D, from which the thermal conductivity was calculated using $\kappa = D \times C_P \times d$, where C_P is the Dulong Petit heat capacity, and d is the geometrical density. One should consider that the Dulong–Petit heat capacity may lead to overestimation of the thermal conductivity, especially at high temperatures.

Electronic structure calculations

First-principles electronic structure calculations were performed by using the all-electron, full-potential local orbital (FPLO) method.[29] Because the 4f electrons of Yb give rise to states with narrow band widths, local spin density approximation to the density functional theory had to be augmented by employing the so-called LSDA + U formalism.[30,31] The value of the on-site Coulomb repulsion, U, was taken as 8 eV, a typical value for the 4f electrons in the FPLO package.[32] For the double counting correction, the fully-localized or atomic limit was applied. Brillouin zone integrations were handled by the linear tetrahedron method with a mesh of 12 × 4 × 20.

Besides the standard band structure analysis using density of states (DOS) and electron energy band dispersions, chemical bonding was investigated in real space by a combined electron density – electron localizability indicator (ED-ELI) approach. This approach is based on Bader's quantum theory of atoms in molecules (QTAIM).[33] The topological analysis of ELI provides information regarding the nature of bonds (two- or multi-centered, number of electrons participating in the bond), lone-pair-like features and core shells.[34,35] The basin intersection technique allows identification of individual atom contributions to the electron populations of the bond basins.[36] The ED and ELI were calculated using a module implemented in the FPLO package.[37] The topological analysis and the basin intersection calculations were carried out by the program DGRID.[38]

Results and discussion

Phase analysis

$Yb_5Al_2Sb_6$ was originally obtained by Todorov *et al.* as a by-product during the solid state synthesis of YbAlSbGe.[25] Their attempts to prepare $Yb_5Al_2Sb_6$ as a single phase from the stoichiometric mixture of the elements failed, and eventually they suggested that a small amount of Ge was required in the reaction. It was proposed that Ge might act as a catalyst or form a low-temperature eutectic, which prevents formation of binary phases of Yb and Sb. In our studies, we found that the $Yb_5Al_2Sb_6$ sample prepared from the stoichiometric amount of elements contained more than 5 wt% Yb_5Sb_3 as a secondary phase. This might indicate that during the synthesis process, some Al might be lost or the phase is stabilized with higher Al content. Therefore, in the next iteration, the sample was prepared with excess Al (0.65 at%, corresponding to $Yb_5Al_{2.1}Sb_6$). In this way, $Yb_5Al_2Sb_6$ was obtained in very high yield with less than 2 wt% Yb_5Sb_3 as a secondary phase (Fig. 2). $Yb_5Ga_2Sb_6$ and $Yb_5In_2Sb_6$ were previously prepared by either metal flux

 This journal is © The Royal Society of Chemistry 2015

Published on 02 February 2015. Downloaded by California Institute of Technology on 14/01/2016 23:12:30.

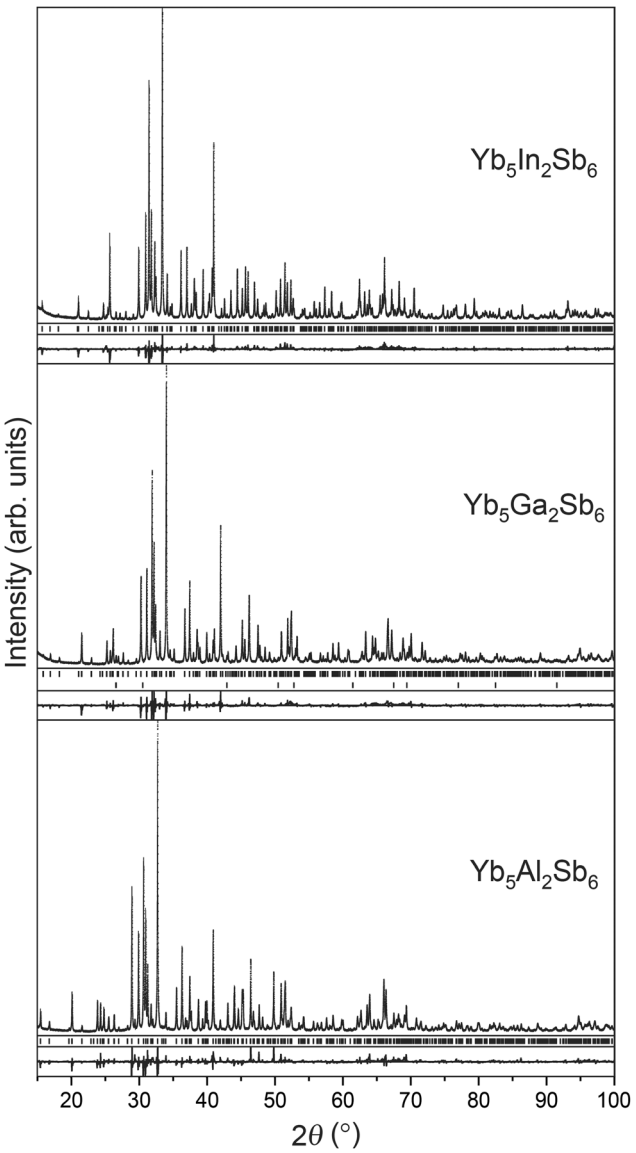

Fig. 2 The Rietveld fit of $Yb_5M_2Sb_6$ samples (R_i, R_p, R_{wp}: 0.07, 0.15, 0.14; 0.04, 0.14, 0.12; 0.06, 0.12, 0.12 for M = Al, Ga, and In, respectively. All reflections of the main phases could be indexed using the reported crystal structure data.[23–25] For the middle panel, the upper and lower ticks mark the calculated reflection positions of $Yb_5Ga_2Sb_6$ and GaSb,[39] respectively, and for others the ticks show the calculated reflection position of the target phases. The difference profiles are shown beneath of each panel.

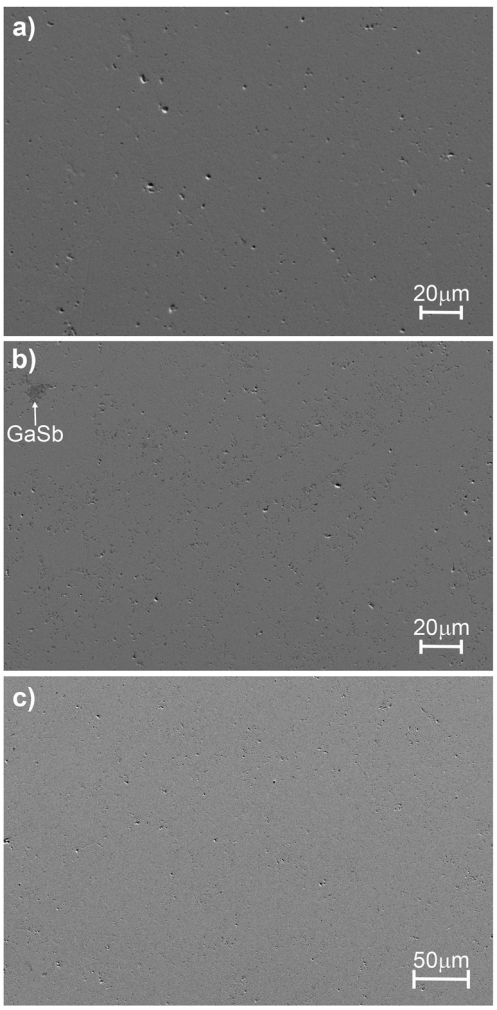

Fig. 3 SEM images of (a) $Yb_5Al_2Sb_6$, (b) $Yb_5Ga_2Sb_6$ and (c) $Yb_5In_2Sb_6$ in secondary electron imaging mode show homogenous microstructure and high density. The secondary phase of GaSb is marked for $Yb_5Ga_2Sb_6$.

technique or solid state reaction of the elements.[23,24] In this investigation, after ball-milling followed by hot-pressing, they were obtained in very high yield with less than 1–2 wt% GaSb or InSb as by-products (Fig. 2).

The SEM images in secondary electron imaging mode are shown in Fig. 3. Hot-pressed samples show almost homogenous microstructures with no noticeable grain boundaries. The secondary phase of GaSb is marked for the $Yb_5Ga_2Sb_6$ sample. This impurity phase appears to be distributed in the grains of the main phase, rather than precipitating at possible grain boundaries. The chemical compositions of the $Yb_5Ga_2Sb_6$ and $Yb_5In_2Sb_6$ samples were determined by EDXS as $Yb_{4.97}Ga_{2.03}Sb_{6.01}$ and $Yb_{5.02}In_{1.99}Sb_{5.99}$, respectively. The determination of the chemical composition of $Yb_5Al_{2.1}Sb_6$ phase was hindered by the overlapping Yb–M and Al-Kα energy levels (1.486 and 1.521 eV, respectively). Taking that into consideration, WDXS analysis revealed a composition of $Yb_{4.72(5)}Al_{2.40(9)}Sb_{5.88(6)}$, indicating an Al-excess composition. The composition was determined additionally by Rietveld refinement as $Yb_{4.82}Al_{2.38}Sb_{5.98}$, which is similar to the microprobe result. This may suggest that an Al-rich composition is stable, explaining why a higher concentration of Yb_5Sb_3 was observed in the sample with a synthetic composition of $Yb_5Al_2Sb_6$, compared with $Yb_5Al_{2.1}Sb_6$.

Crystal structure

As discussed above, $Yb_5M_2Sb_6$ compounds crystallize in the $Ca_5Al_2Bi_6$ structure type comprising $^1_\infty(M_2Sb_6)^{10-}$ double chains separated by Yb atoms (Fig. 4a). In this crystal struc-

Published on 02 February 2015. Downloaded by California Institute of Technology on 14/01/2016 23:12:30.

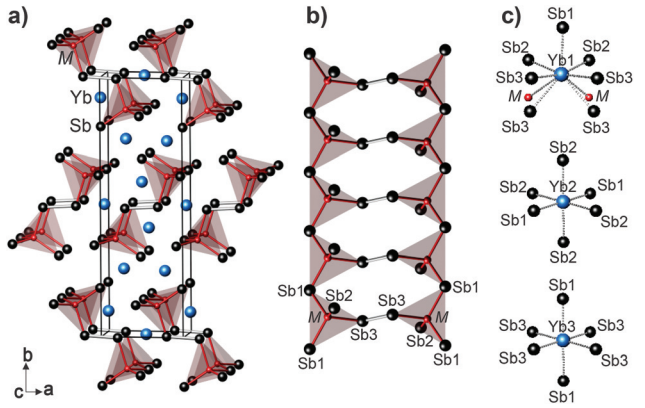

Fig. 4 (a) The crystal structure of $Yb_5M_2Sb_6$ (M = Al, Ga, and In) compounds crystallizing in the orthorhombic unit cell. (b) Infinite double chains $^1_\infty(M_2Sb_6)^{10-}$ formed by Sb3–Sb3 bridging of MSb_4 tetrahedra. (c) Local environments of Yb atoms.

ture, single chains are formed by corner-sharing MSb_4 tetrahedra, which are further bridged by Sb3 atoms to form double chains (Fig. 4b). It was previously reported that depending on the cation size *e.g.*, Ba or Ca, dimeric anion $(M_2Sb_6)^{12-}$ or polymeric chains of $^1_\infty(MSb_6)^{3-}$ may also form, as in Ba_3AlSb_3 or Ca_3AlSb_3, respectively.[17,40–42] In this case, the $^1_\infty(M_2Sb_6)^{10-}$ double chain can be considered to be obtained by removing one Ca from the crystal structure of Ca_3AlSb_3 ($Ca_6Al_2Sb_6$) which leads to oxidative coupling of Sb–Sb bonds in (Al_2Sb_6).[25]

The $Yb_5M_2Sb_6$ compounds crystallize in the orthorhombic unit cell *Pbam* (no. 55), with lattice parameters given in Table 1. Currently refined lattice parameters for M = Ga and In are very close to the previously reported ones. In case of M = Al, our refinement gives values close to the ones reported by Fornasini *et al.*,[43] but substantially different than the ones reported by Todorov *et al.*,[25] which needs further clarification. In the crystal structure of $Yb_5M_2Sb_6$, there are 3 × Yb (Yb1, Yb2: 4 g (*x*, *y*, 0); Yb3: 2*a* (0, 0, 0)), 1 × M (4 h (*x*, *y*, 1/2)) and 3 × Sb (Sb1: 4 g (*x*, *y*, 0); Sb2, Sb3: 4 h (*x*, *y*, 1/2)) positions. During the Rietveld refinements (see Fig. 2), all the atomic positions were refined with full occupancy. In $Yb_5M_2Sb_6$, MSb_4 tetrahedral distances vary from 2.59–2.81 Å for Al, from 2.70–2.84 Å for Ga and 2.81–2.95 Å for In, in accordance with the increase in the atomic radius down the group III elements. The bridging Sb3–Sb3 distances on the other hand remain almost constant (2.93–2.95 Å). Similar behaviour is observed in the $Ae_5In_2Sb_6$ (Ae = Ca, Sr, Ba) series where the Sb–Sb distances do not change even if the cation size changes dramatically.[15,44,45] This may indicate that the space requirement is fulfilled by changing the size of the MSb_4 tetrahedra and relaxing the corresponding angles among the M and Sb atoms. While Yb1 atoms have 7 × Sb and 2 × M atoms as nearest neighbours, Yb2 and Yb3 atoms form an almost regular octahedral arrangement with 6 × Sb atoms (Fig. 4c; interatomic distances of Yb1: 3.21–3.49 Å, 3.20–3.50 Å, and 3.25–3.59 Å; Yb2: 3.16–3.22 Å, 3.17–3.21 Å and 3.20–3.23 Å; Yb3: 3.11, 3.11, and 3.16 Å; for M = Al, Ga and In, respectively).

Table 1 The lattice parameters (Å) of currently investigated samples and previously reported ones

Compds.	Lattice Param.	Reported lattice Param.	Ref.
$Yb_5Al_2Sb_6$	*a* = 7.3234(7)	*a* = 7.321(2); 7.2971(15)	43 and 25
	b = 22.877(2)	*b* = 22.878(4); 22.780(5)	
	c = 4.4099(4)	*c* = 4.4061(4); 4.4115(9)	
$Yb_5Ga_2Sb_6$	*a* = 7.2864(7)	*a* = 7.2769(2)	24
	b = 22.902(2)	*b* = 22.9102(5)	
	c = 4.4020(5)	*c* = 4.39840(10)	
$Yb_5In_2Sb_6$	*a* = 7.3950(7)	*a* = 7.3992(5)	23
	b = 22.985(1)	*b* = 23.001(6)	
	c = 4.5119(2)	*c* = 4.5139(4)	

The electronic band structure and chemical bonding

The electronic DOS calculated for the title compounds are presented in Fig. 5. The top panels show the total DOS with the 4f contributions subtracted. The sharply peaked 4f states (not shown for clarity purposes) are mainly located between −2.5 and −2.0 eV in all cases. The middle (bottom) panels show the s (p) partial DOS of the Sb1, Sb2, Sb3 and the M atoms. The overall behavior observed in these figures are very similar for all three compounds. The occupied states are grouped in three energy ranges with approximate boundaries (a) −11 to −8 eV, (b) −5.5 to −4.5 eV (M = Al, In) or −6.5 to −5 eV (M = Ga), (c) −4.5 to 0 (Fermi energy) eV. The energy range −8, −11 eV is dominated by Sb s contributions, while somewhat smaller M atom p and s states also show up. The states of group (b) are mainly dominated by M atom s and Sb p contributions. These hybridizations are expected to take part in the M-Sb bonds of the MSb_4 tetrahedra. The group (a) and group (b) states have band gaps of 2.8, 2.0 and 2.3 eV for M = Al, Ga and In, respectively. The band gaps between group (b) and (c) states are, on the other hand, 0.03, 0.6 and 0.4 eV for M = Al, Ga and In, respectively. The group (c) states are composed of Sb and M p states; the Yb 5d states (not shown) are sizeable only in the interval (−2.5, −0.5) eV with maximum values around 1 states eV^{-1} per spin. Sb1, Sb2, M p partial DOS and all Yb 5d partial DOS display a pseudogap behavior between Fermi energy and 1 eV, but Sb3 5p state contributions do not go to zero, rather they stay constant around 0.6 states eV^{-1} per spin (with the exception of some peaks). The Sb3 atoms form the Sb–Sb dimers bridging the MSb_4 tetrahedra. The different behavior of the Sb3 5p states in this energy range may reflect the Sb3–Sb3 two-center bonds detected in the ELI analysis (see below) and the metallic nature of the DOS owes the most to these states.

According to the topological analysis of the electron density, ED, Al loses about 1.2 electrons and In about 0.2, whereas Ga is almost neutral. In all cases and for all symmetry types of Yb atoms, the 4f occupancy was found to be 14, suggesting a +2 valence. However, the calculated electron populations of the Yb atoms show that each Yb atom contributes a total of 0.8–0.9 electrons to the ELI bond basins. The topological analysis of the ELI reveals that the expected bonding situation in the $Yb_5M_2Sb_6$, M = Al, Ga, In compounds is realized only for the M = Al case. The ELI distribution

 This journal is © The Royal Society of Chemistry 2015

Published on 02 February 2015. Downloaded by California Institute of Technology on 14/01/2016 23:12:30.

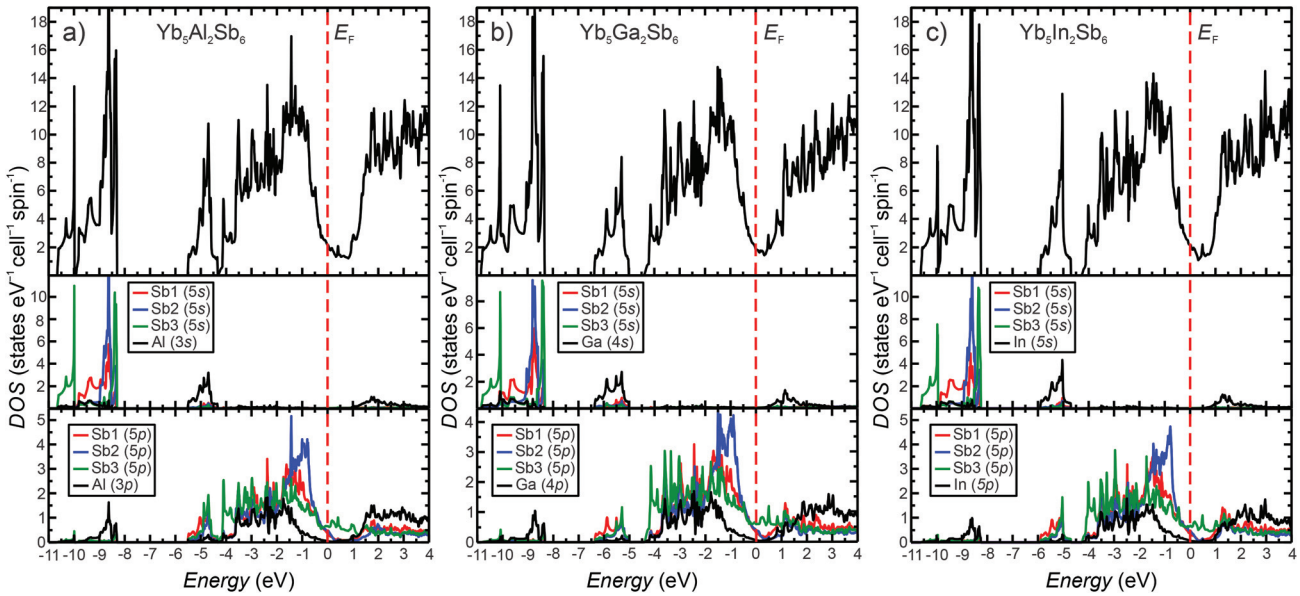

Fig. 5 Total and partial density of states of $Yb_5M_2Sb_6$ (M = Al, Ga, In) compounds. The vertical dashed line stands for the Fermi level.

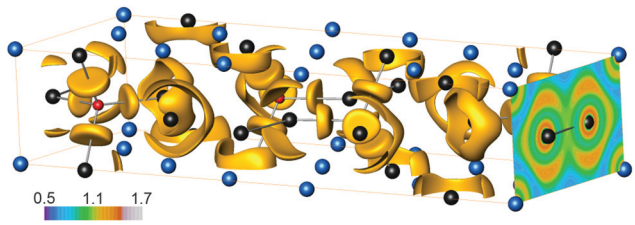

Fig. 6 Distribution of the electron localizability indicator in $Yb_5Al_2Sb_6$ (Yb: blue; Al: Red; Sb: black). The positions of the ELI maxima reflecting the Ga–Sb and Sb–Sb bonds and the 'lone pairs' are visualized by the isosurfaces with $\Upsilon = 1.25$.

obtained for $Yb_5Al_2Sb_6$ is displayed in Fig. 6 using an isosurface value of $\Upsilon = 1.25$. The Sb–Al two-center bonds and the lone-pair like features of the Sb atoms are all separate. The basin intersection analysis shows that Sb contributions are about 3–4 times that of Al. The basins corresponding to the lone pairs of the Sb atoms contain Yb contributions between 5 and 10% of the total basin electron populations. In contrast, in $Yb_5Ga_2Sb_6$ the Sb–Ga bond and lone pair attractors merge into a single attractor for the Sb3 symmetry type, while they remain separated for Sb1 and Sb2. In $Yb_5In_2Sb_6$ the attractors merge for both Sb1 and S3. Although the bond and lone pair attractors are separate for Sb2, there are contributions from the In atoms to the basins of the lone pairs at the level of Yb contributions, namely about 5–10 per cent. The Sb3–Sb3 bond, found in all cases, has an electron population of 0.4, and a lower attractor value, $Y = 1.08$–1.09, than the Sb–M and lone pair attractors.

Electronic transport

The $Yb_5M_2Sb_6$ structure can be rationalized using the Zintl–Klemm concept as discussed above, suggesting that $Yb_5M_2Sb_6$ compounds might exhibit semiconducting electronic behaviour similar to $Ca_5M_2Sb_6$ compounds. However, as predicted by DFT calculations, the electronic transport measurements of $Yb_5M_2Sb_6$ compounds reveal metallic behaviour, rather than semiconducting. As illustrated by Fig. 7a, $Yb_5M_2Sb_6$ compounds have very high p-type carrier concentrations on the order of 5×10^{21} h^+ cm^{-3}. The resistivity and Seebeck coefficients, shown in Fig. 7b and d, are low at room temperature and increase linearly with increasing temperature. The Hall mobility (Fig. 7c) is similar in magnitude to that observed in other $A_5M_2Sb_6$ compounds, and it decreases with temperature as expected when acoustic phonons are the primary scattering source. These results in $Yb_5Al_2Sb_6$ and $Yb_5In_2Sb_6$ are consistent with previous reports of metallic electronic conductivity.[23,25] The Seebeck coefficients of $Yb_5Al_2Sb_6$ in the current study are identical to those reported by Todorov *et al.*[25] There are several potential explanations for the observed metallic behaviour: (i) a valence imbalance due to positively charged site defects, (ii) valence imbalance resulting from mixed valence of Yb, or (iii) $Yb_5M_2Sb_6$ compounds are semimetals in which the conduction band minima and valence band maxima overlap, as supported by DFT results. Each of these possibilities is explored below.

Charged point defects are responsible for high carrier concentrations in several well-known thermoelectric materials ($La_{3-x}Te_4$, $Ba_8Ge_{43}\square_3$[46–48]), including AZn_2Sb_2 (A = Sr, Ca, Eu, Yb) Zintl compounds with the $CaAl_2Si_2$ structure type.[49,50] To explain the large observed carrier concentrations in $Yb_5M_2Sb_6$ compounds however, an unrealistically large concentration of point defects would be necessary. For example, if each Yb vacancy yields two holes, then a 15% Yb deficiency would correspond to a carrier concentration of 4×10^{21} h^+ cm^{-3}. Subbarao *et al.* have suggested that Yb is in a mixed 2+/3+ valence state,[24] as observed in several other Zintl phases.[51] However,

Published on 02 February 2015. Downloaded by California Institute of Technology on 14/01/2016 23:12:30.

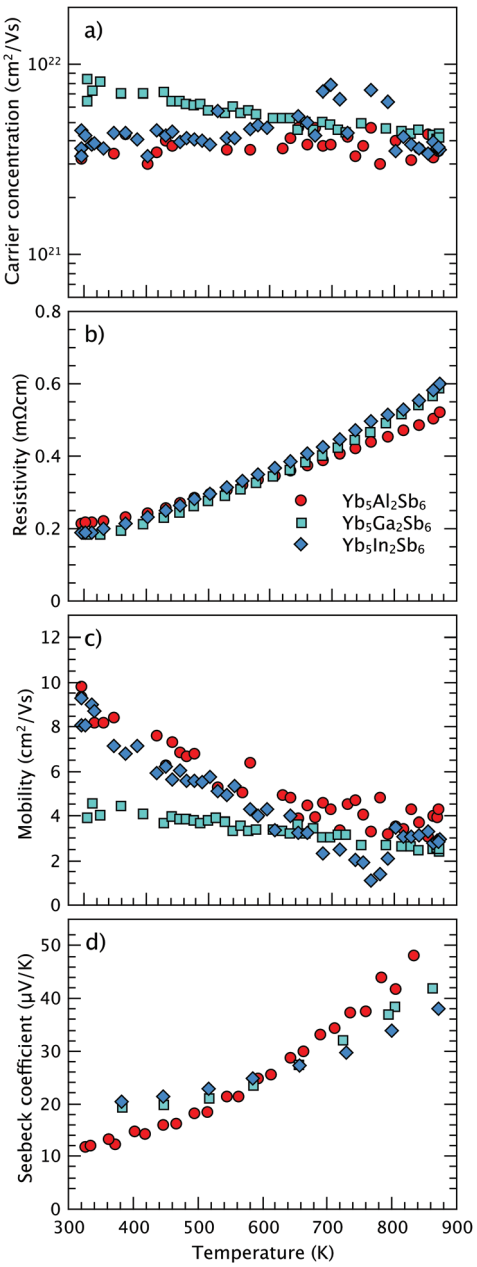

Fig. 7 (a) $Yb_5M_2Sb_6$ compounds exhibit high p-type carrier concentrations with (b) resistivity behaviour characteristic of a semimetal. (c) Hall mobility is comparable to $Ca_5M_2Sb_6$ compounds with a similar structure type. (d) $Yb_5M_2Sb_6$ displays low Seebeck coefficients.

the presence of Yb^{3+} would be expected to lead to n-type behaviour, rather than the observed p-type behaviour.

Finally, as DFT calculations suggest, $Yb_5M_2Sb_6$ compounds may have overlapping valence and conduction bands, leading to semimetallic behaviour. The temperature dependent transport of a semimetal resembles a degenerate (heavily doped) semiconductor, which has a finite band gap. There are, however, a few noticeable differences: for example the Seebeck coefficient for a degenerate semiconductor is 0 at 0 K and increases linearly with temperature, whereas that of a semimetal is often nonlinear (although also passes through the origin). More specifically, for a small overlap $E_g = -0.1$ eV, a semimetal that has large free carrier concentration reveals an upward deviation, whereas a semimetal with low free carrier concentration reveals a downward deviation. The Seebeck coefficient value of a semimetal is also affected by parameters of both the majority carrier band and the minority carrier band (such influence is small when the free carrier concentration is high), whereas for degenerate semiconductors, the minority band usually has negligible influence. The observed temperature dependency of the Seebeck coefficient (Fig. 7d), clearly nonlinear and increasing faster at higher temperatures, can be well explained under the framework of a semimetal with high free carrier concentration, using reasonable material parameters (for example, quantitatively assuming $E_g = -0.1$ eV, $n = 2 \times 10^{21}$ h^+ cm^{-3}, single parabolic band with effective mass of 1 for electrons and 2 for holes, deformation potential coefficient of 15 eV for both, elastic constant $C_l = 150$ GPa). This also explains the large Hall carrier concentration ($1/eR_H$) that is largely temperature independent (Fig. 7a). The Hall mobility is low partly due to the large carrier concentration, and decreases with increasing temperature as a result of phonon scattering (Fig. 7c).

Thermal transport

The total (κ_{total}) and lattice ($\kappa_{Lattice}$) thermal conductivities of the $Yb_5M_2Sb_6$ samples are shown in Fig. 8. The electronic contribution, κ_e, was estimated using the Wiedemann–Franz relation ($\kappa_e = LT/\rho$). Calculating the Lorenz number, L, using a single parabolic band model yields $\kappa_e > \kappa_{total}$, leading to a negative κ_L, indicating that L in these compounds are very poorly described by this model.[52] Consequently, the non-degenerate value, $L = 1.5 \times 10^{-8}$ $W\Omega K^{-2}$, was used to estimate κ_L in Fig. 8. This leads to lattice thermal conductivities ($\sim$ 0.6 W mK^{-1}) at high temperatures that are comparable to κ_L in $Ca_5M_2Sb_6$ compounds.

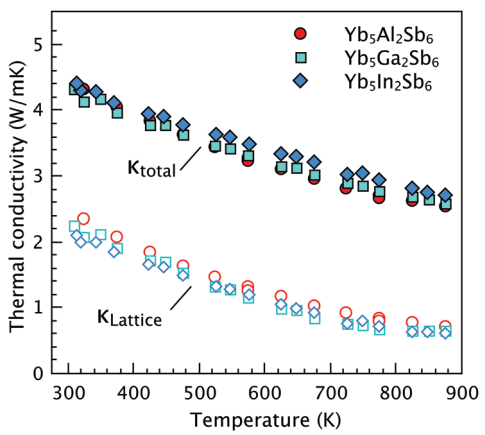

Fig. 8 The total thermal conductivity in $Yb_5M_2Sb_6$ compounds is high due to the large electronic contribution. Subtracting the electronic term (assumes $L = 1.5 \times 10^{-8}$ W Ω K^{-2}) yields lattice thermal conductivities comparable to that of other $A_5M_2Sb_6$ phases.

This journal is © The Royal Society of Chemistry 2015

Published on 02 February 2015. Downloaded by California Institute of Technology on 14/01/2016 23:12:30.

Table 2 Physical properties of $Yb_5M_2Sb_6$ compounds: theoretical density, *d*; shear and bulk modulus, *G* and *K*; transverse and longitudinal sound velocities, ν_T and ν_L

Compounds	d (g cm^{-3})	G (GPa)	K (GPa)	ν_T (m s^{-1})	ν_L (m s^{-1})
$Yb_5Al_2Sb_6$	7.47	28.4	39.4	1950	3215
$Yb_5Ga_2Sb_6$	7.68	26.5	34.9	1860	3025
$Yb_5In_2Sb_6$	7.89	25.2	34.1	1785	2930

Table 2 shows the sound velocities and elastic moduli of $Yb_5M_2Sb_6$ compounds, obtained from ultrasonic measurements. The sound velocity in a solid is related to the material's density, d, and stiffness, E, by the general expression $\nu \propto \sqrt{E/d}$. In $Yb_5M_2Sb_6$, the transition towards heavier triel elements (Al, Ga, In) leads to increased theoretical density, decreased lattice stiffness, and a corresponding decrease in the speed of sound. Compared with the $Ca_5M_2Sb_6$ series, the speeds of sound in $Yb_5M_2Sb_6$ compounds are approximately 20% lower, which implies that κ_L in the Yb-based compounds should also be lower. However, the large electronic thermal conductivity in these compounds makes it difficult to accurately compare the lattice thermal conductivities.

Figure of merit

The $Yb_5M_2Sb_6$ compounds have similar figure of merit, zT, values (Fig. 9). The low zT values (<0.15) are attributable to the metallic electronic properties of the samples. A band gap between bonding and anti-bonding states is necessary for good thermoelectric performance because it allows for a single carrier type to dominate transport.[53] In a semimetal, the two competing carrier types will always lead to low, compensated Seebeck coefficients. Efforts to increase the zT in these compounds should thus be directed at opening a band gap and increasing its magnitude, perhaps through substitutions on the cation or pnictogen site.

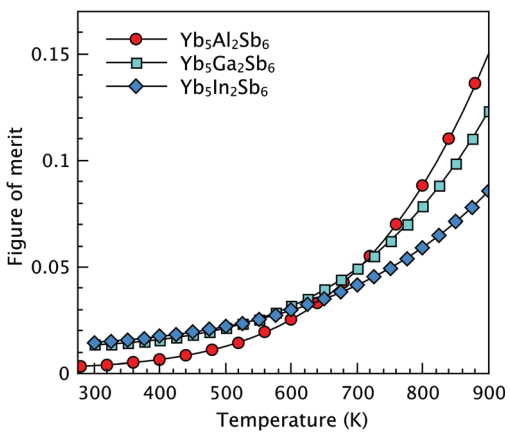

Fig. 9 The figures of merit of $Yb_5M_2Sb_6$ compounds are lower than 0.15 due to semimetallic transport behaviour.

Conclusions

Zintl compounds of $Yb_5M_2Sb_6$ (M = Al, Ga, and In) were obtained in very high yield by ball milling followed by hot pressing. The band structure calculations revealed finite density of states at the Fermi level implying metallic behaviour. High temperature thermoelectric properties measurements show that all three compounds have relatively low electrical resistivity, low Seebeck coefficients and high total thermal conductivities in agreement with the calculations. Consequently, the thermoelectric figures of merit of all compounds remain relatively low, less than 0.15, in the whole temperature range investigated.

Acknowledgements

U. A. greatly acknowledges the financial assistance of The Scientific and Technological Research Council of Turkey. This research was partially carried out at the Jet Propulsion Laboratory, California Institute of Technology, under a contract with the National Aeronautics and Space Administration and was supported by the NASA Science Missions Directorate's Radioisotope Power Systems Technology Advancement Program. A. O. thanks Ulrike Nitzsche from IFW Dresden, Germany for technical help in computational work.

Notes and references

1 G. J. Snyder and E. S. Toberer, *Nat. Mater.*, 2008, **7**, 105–114.
2 F. J. DiSalvo, *Science*, 1999, **285**, 703–706.
3 S. M. Kauzlarich, S. R. Brown and G. J. Snyder, *Dalton Trans.*, 2007, 2099–2107, DOI: 10.1039/b702266b.
4 E. S. Toberer, A. F. May and G. J. Snyder, *Chem. Mater.*, 2010, **22**, 624–634.
5 S. M. Kauzlarich, *Chemistry, Structure, and Bonding of Zintl Phases and Ions*, Wiley-VCH, 1996.
6 E. S. Toberer, A. Zevalkink and G. J. Snyder, *J. Mater. Chem.*, 2011, **21**, 15843–15852.
7 S. K. Bux, A. Zevalkink, O. Janka, D. Uhl, S. Kauzlarich, J. G. Snyder and J. P. Fleurial, *J. Mater. Chem. A*, 2014, **2**, 215–220.
8 S. R. Brown, S. M. Kauzlarich, F. Gascoin and G. J. Snyder, *Chem. Mater.*, 2006, **18**, 1873–1877.
9 U. Aydemir, L. Akselrud, W. Carrillo-Cabrera, C. Candolfi, N. Oeschler, M. Baitinger, F. Steglich and Y. Grin, *J. Am. Chem. Soc.*, 2010, **132**, 10984–10985.
10 C. Candolfi, U. Aydemir, A. Ormeci, W. Carrillo-Cabrera, U. Burkhardt, M. Baitinger, N. Oeschler, F. Steglich and Y. Grin, *J. Appl. Phys.*, 2011, **110**, 043715.
11 C. Candolfi, U. Aydemir, M. Baitinger, N. Oeschler, F. Steglich and Y. Grin, *J. Appl. Phys.*, 2012, **111**, 043706.

Published on 02 February 2015. Downloaded by California Institute of Technology on 14/01/2016 23:12:30.

12 C. Candolfi, U. Aydemir, A. Ormeci, M. Baitinger, N. Oeschler, F. Steglich and Y. Grin, *Phys. Rev. B: Condens. Matter*, 2011, **83**, 205102.
13 S. I. Johnson, A. Zevalkink and G. J. Snyder, *J. Mater. Chem. A*, 2013, **1**, 4244–4249.
14 E. S. Toberer, A. Zevalkink, N. Crisosto and G. J. Snyder, *Adv. Funct. Mater.*, 2010, **20**, 4375–4380.
15 A. Zevalkink, J. Swallow and G. J. Snyder, *Dalton Trans.*, 2013, **42**, 9713–9719.
16 P. Verdier, P. Lharidon, M. Maunaye and Y. Laurent, *Acta Crystallogr., Sect. B: Struct. Crystallogr. Cryst. Chem.*, 1976, **32**, 726–728.
17 G. Cordier, H. Schafer and M. Stelter, *Z. Naturforsch., B: Condens. Matter*, 1984, **39**, 727–732.
18 Y. L. Yan and Y. X. Wang, *J. Mater. Chem.*, 2011, **21**, 12497–12502.
19 Y. L. Yan, Y. X. Wang and G. B. Zhang, *Comput. Mater. Sci.*, 2014, **85**, 88–93.
20 A. Zevalkink, G. S. Pomrehn, S. Johnson, J. Swallow, Z. M. Gibbs and G. J. Snyder, *Chem. Mater.*, 2012, **24**, 2091–2098.
21 A. Zevalkink, J. Swallow and G. J. Snyder, *J. Electron. Mater.*, 2012, **41**, 813–818.
22 A. Zevalkink, E. S. Toberer, T. Bleith, E. Flage-Larsen and G. J. Snyder, *J. Appl. Phys.*, 2011, **110**, 013721.
23 S. J. Kim, J. R. Ireland, C. R. Kannewurf and M. G. Kanatzidis, *J. Solid State Chem.*, 2000, **155**, 55–61.
24 U. Subbarao, S. Sarkar, V. K. Gudelli, V. Kanchana, G. Vaitheeswaran and S. C. Peter, *Inorg. Chem.*, 2013, **52**, 13631–13638.
25 I. Todorov, D. Y. Chung, L. Ye, A. J. Freeman and M. G. Kanatzidis, *Inorg. Chem.*, 2009, **48**, 4768–4776.
26 L. Akselrud and Y. Grin, *J. Appl. Crystallogr.*, 2014, **47**, 803–805.
27 S. Iwanaga, E. S. Toberer, A. LaLonde and G. J. Snyder, *Rev. Sci. Instrum.*, 2011, **82**, 063905.
28 K. A. Borup, E. S. Toberer, L. D. Zoltan, G. Nakatsukasa, M. Errico, J. P. Fleurial, B. B. Iversen and G. J. Snyder, *Rev. Sci. Instrum.*, 2012, **83**, 123902.
29 H. E. K. Koepernik, *Phys. Rev. B: Condens. Matter*, 1999, **59**, 1743–1757.
30 J. P. Perdew and Y. Wang, *Phys. Rev. B: Condens. Matter*, 1992, **45**, 13244–13249.
31 V. I. Anisimov, J. Zaanen and O. K. Andersen, *Phys. Rev. B: Condens. Matter*, 1991, **44**, 943–954.
32 H. Eschrig, K. Koepernik and I. Chaplygin, *J. Solid State Chem.*, 2003, **176**, 482–495.
33 R. F. W. Bader, *Atoms in Molecules: A Quantum Theory*, Clarendon Press, Oxford, 1990.
34 M. Kohout, *Faraday Discuss.*, 2007, **135**, 43–54.
35 F. R. Wagner, V. Bezugly, M. Kohout and Y. Grin, *Chem. – Eur. J.*, 2007, **13**, 5724–5741.
36 S. Raub and G. Jansen, *Theor. Chem. Acc.*, 2001, **106**, 223–232.
37 A. Ormeci, H. Rosner, F. R. Wagner, M. Kohout and Y. Grin, *J. Phys. Chem. A*, 2006, **110**, 1100–1105.
38 M. Kohout, *Program DGRID, Version 4.6*, Radebeul, Germany, 2011.
39 M. E. Straumanis and E. Z. Aka, *J. Appl. Phys.*, 1952, **23**, 330–334.
40 G. Cordier, G. Savelsberg and H. Schafer, *Z. Naturforsch., B: Chem. Sci.*, 1982, **37**, 975–980.
41 W. G. Zeier, A. Zevalkink, E. Schechtel, W. Tremel and G. J. Snyder, *J. Mater. Chem.*, 2012, **22**, 9826–9830.
42 A. Zevalkink, E. S. Toberer, W. G. Zeier, E. Flage-Larsen and G. J. Snyder, *Energy Environ. Sci.*, 2011, **4**, 510–518.
43 M. L. Fornasini and P. Manfrinetti, *Z. Kristallogr. - New Cryst. Struct.*, 2009, **224**, 345–346.
44 G. Cordier, H. Schafer and M. Stelter, *Z. Naturforsch., B: Chem. Sci.*, 1985, **40**, 5–8.
45 G. Cordier and M. Stelter, *Z. Naturforsch., B: Chem. Sci.*, 1988, **43**, 463–466.
46 A. F. May, J.-P. Fleurial and G. J. Snyder, *Phys. Rev. B: Condens. Matter*, 2008, **78**, 125205.
47 U. Aydemir, C. Candolfi, H. Borrmann, M. Baitinger, A. Ormeci, W. Carrillo-Cabrera, C. Chubilleau, B. Lenoir, A. Dauscher, N. Oeschler, F. Steglich and Y. Grin, *Dalton Trans.*, 2010, **39**, 1078–1088.
48 C. Candolfi, U. Aydemir, M. Baitinger, N. Oeschler, F. Steglich and Y. Grin, *J. Electron. Mater.*, 2010, **39**, 2039–2042.
49 G. S. Pomrehn, A. Zevalkink, W. G. Zeier, A. van de Walle and G. J. Snyder, *Angew. Chem., Int. Ed.*, 2014, **126**, 3490–3494.
50 A. Zevalkink, W. G. Zeier, E. Cheng, J. Snyder, J. P. Fleurial and S. Bux, *Chem. Mater.*, 2014, **26**, 5710–5717.
51 J. R. Salvador, D. Bilc, S. D. Mahanti, T. Hogan, F. Guo and M. G. Kanatzidis, *J. Am. Chem. Soc.*, 2004, **126**, 4474–4475.
52 E. Flage-Larsen and O. Prytz, *Appl. Phys. Lett.*, 2011, **99**, 202108.
53 G. D. Mahan, *Solid State Phys.*, 1998, **51**, 81–157.

This journal is © The Royal Society of Chemistry 2015